Readout methods and devices for Josephson-junction-based solid-state qubits

2006 J. Phys.: Condens. Matter 18 S901

(http://iopscience.iop.org/0953-8984/18/21/S14)

INSTITUTE OF PHYSICS PUBLISHING JOURNAL OF PHYSICS: CONDENSED MATTER

J. Phys.: Condens. Matter **18** (2006) S901–S920 doi:10.1088/0953-8984/18/21/S14

Readout methods and devices for Josephson-junction-based solid-state qubits

G Johansson, L Tornberg, V S Shumeiko and G Wendin

Department of Microtechnology and Nanoscience-MC2, Chalmers University of Technology, SE-41296 Gothenburg, Sweden

Received 7 December 2005, in final form 6 February 2006
Published 12 May 2006
Online at stacks.iop.org/JPhysCM/18/S901

Abstract

We discuss the current situation concerning measurement and readout of Josephson-junction based qubits. In particular, we focus attention on dispersive low-dissipation techniques involving reflection of radiation from an oscillator circuit coupled to a qubit, allowing single-shot determination of the state of the qubit. In particular, we develop a formalism describing a charge qubit read out by measuring its effective (quantum) capacitance. To exemplify, we also give explicit formulas for the readout time.

(Some figures in this article are in colour only in the electronic version)

1. Introduction

Nanotechnology is considered promising for fabrication of scalable solid-state electronics for quantum computers [1–3]. However, progress towards solid-state quantum computing will critically depend on the development of measurement schemes and readout devices that, on demand, can determine the state of individual qubits in a fraction of the coherence time, but which otherwise do not disturb the qubit system. In quantum optics, efficient measurement techniques have been developed during the last 30 years based on laser–atom interactions and recently implemented in e.g. ion traps [4–9].

The corresponding work for solid state systems effectively started only about ten years ago, and is currently exploring various paths. A problem is that there is no general device for operation and readout, like a laser, but rather a multitude of implementations of measurements of charge, spin, magnetic flux and charge current that must be adapted to the specific qubits to be studied. Therefore, the qubit readout technology must be developed in intimate connection with the qubits for characterization and control of coherence properties. This is a painstakingly slow process, which, however, cannot be circumvented, because it is essential in many respects. In particular, it is an important tool for determining the coherence properties of the qubits. Moreover, the technology not only concerns qubit readout devices, but also involves quantum oscillators for storing and transmitting information and for coupling qubits.

Interestingly enough, quantum-optical methods are now being applied to solid-state qubit systems, using microwaves for operating and reading out qubits, and oscillator circuits and transmission lines for coupling qubits, introducing cavity-QED in solid-state systems [10–12]. This may turn out to be a major road on the Road Map for quantum coherent systems ('quantum computers') [13, 14], and will be at the focus of the present paper. In particular, we will describe some practical schemes for reflecting microwaves from an oscillator circuit, the phase shift measuring the changes in charge [15, 16] or magnetic flux [17–21] induced by a qubit, allowing us to distinguish between the different states $|0\rangle$ and $|1\rangle$ of the qubit.

2. Measurement of quantum information and qubit readout

2.1. Introduction

The ultimate objective of a qubit readout device is to distinguish the *eigenstates* of a qubit in a single measurement 'without destroying the qubit', a so called 'single-shot' quantum non-demolition (QND) projective measurement. This objective is essential for several reasons: state preparation for computation, readout for error correction during the calculation, and readout of results at the end of the calculation. Strictly speaking, the QND property is only needed if the qubit must be left in an eigenstate after the readout. In a broader sense, readout of a specific qubit must of course not demolish other qubits in the system.

Note that one cannot 'read out the *state* of a qubit' in a single measurement—this is prohibited by quantum mechanics. The effect of a single ideal measurement on a qubit in a general superposition $a\,|0\rangle + b\,|1\rangle$ is to leave the qubit in one of the states $|0\rangle$ or $|1\rangle$, which carries no information about the amplitudes a or b. It takes repeated measurements on a large number of replicas of the quantum state to characterize the state of the qubit—'quantum tomography'. This is the procedure to collect the statistics for expectation values.

The measurement connects the qubit with the open system of the detector, which collapses the combined system of qubit and measurement device to one of its common eigenstates. If the coupling between the qubit and the detector is weak, the eigenstates are approximately those of the qubit. In general, however, one must consider the eigenstates of the total qubit-detector system and manipulate gate voltages and fluxes such that the readout measurement is performed in a convenient energy eigenbasis (see e.g. [22] and [23]).

2.2. Survey of readout methods for JJ-based qubits

Here we will provide a brief recapitulation of the 'history' of readout of Josephson-junction-(JJ-) based quantum circuits and qubits. For an extensive discussion of JJ-based qubit circuits, see the recent review by Wendin and Shumeiko [3].

Figure 1 shows general designs for the charge and flux qubits and with oscillator-type readout circuits. The single Cooper-pair box (SCB) (similar to figure 1, left) is described by the Hamiltonian

$$\hat{H} = E_{\mathrm{C}}(n - n_{\mathrm{g}})^2 - E_{\mathrm{J}} \cos\phi \tag{1}$$

and the rf-SQUID (similar to the flux qubit in figure 1, right; see section 6) by the Hamiltonian

$$\hat{H} = E_{\mathrm{C}}\, n^2 - E_{\mathrm{J}}\, \cos\phi + E_{\mathrm{L}} \frac{(\phi - \phi_e)^2}{2}; \tag{2}$$

where E_{C} is the charging energy of the SCB island, E_{J} is the Josephson energy due to Cooper-pair tunnelling between the superconducting electrode and island across the JJ, and E_{L} is the inductive energy of the superconducting loop. n and ϕ are operators for the induced charge and

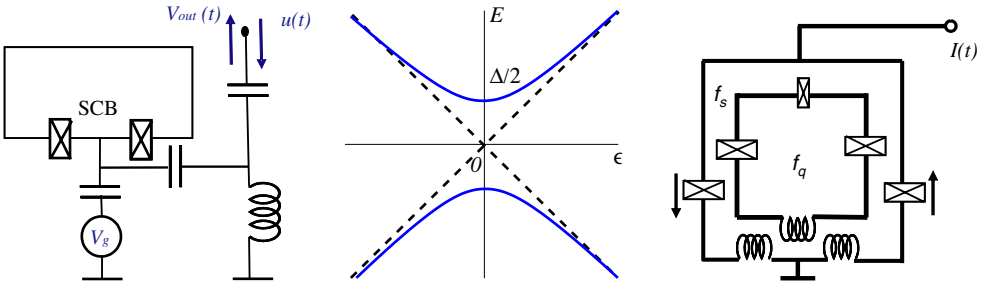

Figure 1. Circuit diagrams and two-level energy spectrum of two basic JJ-qubit designs: the SCB charge qubit with LC-oscillator readout (left), and persistent-current flux qubit with SQUID oscillator readout (right). For the charge qubit, the control variable ϵ on the horizontal axis of the energy spectrum (middle) represents the external gate voltage (induced charge), and the splitting is given by the Josephson tunnelling energy mixing the charge states. For the flux qubit, the variable ϵ represents the external magnetic flux. In both cases, the energy of the qubit can be 'tuned' and the working point controlled. Away from the origin (asymptotically) the levels represent pure charge states (zero $|0\rangle$ or one $|1\rangle$ Cooper pair on the SCB island) or pure flux states (left $|0\rangle$ or right $|1\rangle$ rotating currents in the SQUID ring).

the phase of the (effective) Josephson junction, and n_g is the induced charge controlled by the external bias voltage V_g. Both qubits are represented by the generic two-level Hamiltonian

$$\hat{H} = -\tfrac{1}{2}(\epsilon\sigma_z + \Delta\sigma_x) \tag{3}$$

where σ_z and σ_x are the usual Pauli matrices.

In the original experiment of Nakamura *et al* [24], demonstrating coherent oscillation of the charge qubit two-level system (figure 1, left), the readout was implemented simply by a control dc-pulse on the charge gate, moving the working point far away from the origin so that the upper $|1\rangle$ level ended up above the gap edge of a superconducting lead connected to the SCB island via a tunnel junction. As a result, a Cooper pair on the upper level $|1\rangle$ would immediately decay into the external lead as two quasiparticles, creating a normal electron current. Repeating the measurement at a high rate created a detectable current proportional to the occupation of the upper state $|1\rangle$, revealing the oscillations. Since the SCB is permanently connected to the environment via a tunnel junction, it seemed plausible at the time that this might be the reason for the short coherence time, ∼2–3 ns.

This focused the interest on more advanced readout devices. A remedy could be to use a charge measuring device that was only capacitively coupled to the SCB island and could be turned on and off by an external voltage pulse. Delsing and co-workers [25] therefore developed an rf-SET (radio frequency single-electron transistor) readout [26] for the charge qubit, and successfully detected free oscillations and studied the detailed behaviour of relaxation and dephasing [25]. The result showed that the coherence time was confined to below 10 ns and seemed limited by relaxation effects. Moreover, subsequent experiments by the NEC group [27], implementing more advanced readout concepts, storing the emitted pair of quasiparticles on a superconducting island, and reading the charge with a superconducting SET, made no big change. All in all, the status seems to be that the coherence time of the circuit is severely limited by intrinsic charge fluctuation processes (noise) in the substrate, or in the tunnel barriers, or by transients due to the pulsed operation of the qubit.

Alternatively one could create a new type of charge qubit by connecting the Cooper pair box island to two JJ tunnel junctions, creating a single Cooper pair transistor (SCT). This could be probed via charge [16] or current [28–31] measurements. These experiments can be

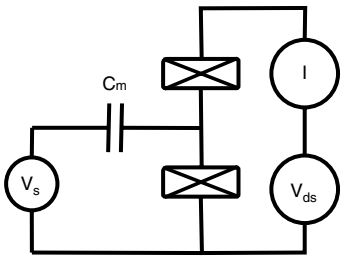

Figure 2. A single-electron transistor: a small metallic island connected to source and drain leads through tunnel junctions. The signal voltage V_s induces a charge q_m on the measurement capacitance C_m. When the system is at the limit of being Coulomb blockaded, a small change of q_m will have a large effect on the current I through the SET.

designed either as threshold detection measurements or as microwave-reflection measurements. The reflection measurements with phase-shift detection will be the main theme of this paper.

Moreover, there is the persistent-current flux qubit, based on a quantum version of the RF-SQUID [33–36] coupled to a measurement dc-SQUID. This measurement SQUID can be operated either as a current threshold detector [35, 36] or as resonance circuit reflecting and phase-shifting microwave radiation [20, 21]. We will also briefly describe the microwave reflection measurement in this case in section 6.

3. Charge measurements

The most straightforward way to read out a charge qubit is to measure its charge. As discussed above, to obtain a high fidelity read-out one should perform a measurement in the qubit eigenbasis. This removes the possibility for the qubit to switch its state during the measurement. When the measurement basis is fixed, as determined by a charge measurement, we need to bias the qubit where the charge basis is the eigenbasis. For the superconducting charge qubit this implies a complete quenching of the Josephson energy, while for quantum dot charge qubits one needs to raise the tunnel barrier between the dots. Having quenched the transitions between the charge states the fidelity will in theory be perfect, irrespectively of the measurement speed. In reality there is always some remaining transition/relaxation channel open which implies the need of a fast read-out. Fast read-out is also mandatory for implementing an error correcting algorithm, where the read-out and correction should be performed on a timescale set by decoherence of the other qubits.

3.1. The radio-frequency single-electron transistor

The state of the art charge measurement device is the radio-frequency single-electron transistor (rf-SET) [26] with an experimentally measured sensitivity of $\delta q = 3.2 \times 10^{-6} e\ \mathrm{Hz}^{-1/2}$ [37]. The measurement time t_{ms} needed to separate two states with a charge difference ΔQ is $t_{ms} = (2\delta q/\Delta Q)^2$, indicating the possibility of detecting a charge difference of one percent of the electron charge ($\Delta Q = 0.01e$) in half a microsecond.

The single-electron transistor (SET) consists of a small metallic island connected to source and drain leads through tunnel junctions (see figure 2). Applying a source–drain voltage the current through the SET depends critically on the charge induced on the gate capacitance. The charge on the gate capacitance is determined by measuring the current. The SET is in itself a sensitive electrometer but suffers from low operating speed, which in addition to being a

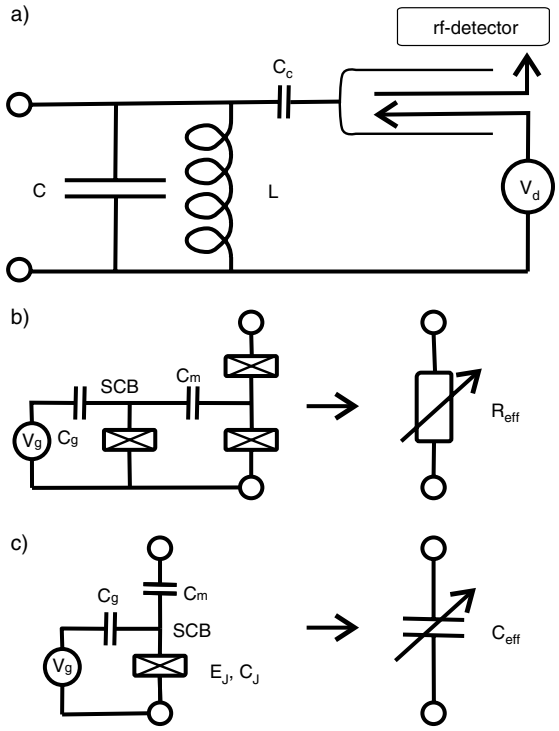

Figure 3. Resonant circuits for read-out: (a) a lumped element LC-oscillator coupled to a driving source and a radio-frequency detector through a transmission line. (b) The radio-frequency single-electron transistor measuring the charge of a charge qubit (SCB). The current through the SET determines the dissipation in the resonant circuit. The dissipation is determined by measuring the amplitude of the reflected signal. (c) Set-up for measuring the quantum capacitance of the charge qubit. The qubit capacitance influences the resonance frequency of the oscillator. The capacitance is measured by determining the phase-shift of the reflected signal.

drawback on its own makes it sensitive to the low frequency charge fluctuations. The rf-SET is realized by embedding an SET in a resonant circuit (see figures 3(a), (b)). The main source of dissipation in the oscillator is current flowing through the SET, and for small amplitude oscillations we may replace the SET by its effective (differential) resistance. The oscillator is excited by sending down a radio-frequency signal on resonance. The dissipation is determined by measuring the amplitude of the reflected signal. This way of operating the SET increases its operating speed and sensitivity significantly.

3.2. Single-shot read-out

The high sensitivity can be used to couple the rf-SET weakly to the charge qubit, reducing the back-action in the off-state. In practice it is impossible to switch off the interaction completely, i.e. the qubit eigenbasis is not exactly the charge basis, and there is some unavoidable mixing of the charge states. A careful investigation of the rf-SET coupled to a superconducting charge qubit shows that single-shot read-out with a very high fidelity is still possible in practice [38–40]. To optimize the fidelity one should bias the charge qubit as far away from the degeneracy point as possible, in order to minimize the effect of any residual Josephson coupling.

4. Capacitance measurements—a quasiclassical description

The low-frequency charge fluctuations present in all realizations of superconducting charge qubits so far [41, 42] promote the use of schemes where the charge qubits are operated at the charge degeneracy point around the origin in figure 1 (middle panel). Here the qubit eigenstates have equal average charge and thus they are shielded from charge fluctuations. To use the rf-SET read-out described in the previous section one needs to quickly shift the qubit far away from degeneracy simultaneously with switching on the measurement. Although this timing is far from impossible, the present trend is to use schemes where the qubit also remains at charge degeneracy during read-out in order to minimize decoherence. This can be achieved by measuring the effective capacitance of the charge qubit, as we describe below.

4.1. Quantum capacitance of a single-Cooper-pair box

The quantum capacitance of the Cooper-pair box [43, 44] is related to the parametric capacitance of small Josephson junctions [45–47], which is a dual to the Josephson inductance. The origin of the quantum capacitance of a single-Cooper-pair box (SCB) can be understood as follows. Assume that we put a constant voltage $V_{\rm m}$ on the measurement capacitance of the SCB, i.e. we put a voltage source between the open circles in figure 3(c). The amount of charge on the measurement capacitance $q_{\rm m}^{\rm g/e}(V_{\rm m}, V_{\rm g})$ will be a nonlinear function of the voltage $V_{\rm m}$ as well as the gate voltage $V_{\rm g}$ and whether the qubit is in the ground or excited state. We may define an effective (differential) capacitance

$$C_{\rm eff}^{\rm g/e}(V_{\rm m}, V_{\rm g}) = \frac{\partial}{\partial V_{\rm m}} q_{\rm m}^{\rm g/e}(V_{\rm m}, V_{\rm g}), \tag{4}$$

as seen from the measurement circuitry. Away from the charge degeneracy points of the SCB no charge will float across the Josephson junction and the effective capacitance is simply the geometric capacitance $C_{\rm geom} = C_{\rm J}C_{\rm m}/(C_{\rm J} + C_{\rm m})$ of the Josephson junction capacitance $C_{\rm J}$ and the measurement capacitance $C_{\rm m}$ in series. Around the charge degeneracy point a change of voltage will induce a shift of a Cooper pair across the Josephson junction. For a voltage changing slowly on the timescale of the inverse qubit gap $\hbar E_{\rm J}^{-1}$ this charge redistribution is dissipationless. This contribution to the effective capacitance, which depends on the qubit state, we call the quantum capacitance $C_{\rm Q}^{\rm g/e}$. From the SCB Hamiltonian (see e.g. equation (18)) it is straightforward to show

$$\begin{aligned} C_{\rm eff}^{\rm g/e}(V_{\rm m}, V_{\rm g}) &= \frac{C_{\rm J}C_{\rm m}}{C_{\rm J} + C_{\rm m}} \pm \frac{C_{\rm m}^2}{C_\Sigma} \frac{E_{\rm J}^2 E_{\rm Q}}{\left(E_{\rm Q}^2[1 - 2(n_{\rm g} + n_{\rm m})]^2 + E_{\rm J}^2\right)^{3/2}} \\ &= C_{\rm geom} + C_{\rm Q}(n_{\rm g} + n_{\rm m}), \end{aligned} \tag{5}$$

where $C_\Sigma = C_{\rm J} + C_{\rm m} + C_{\rm g}$ is the total island capacitance, $E_{\rm Q} = 2e^2/C_\Sigma$ is the Coulomb energy of a Cooper pair, and $n_{\rm g/m} = C_{\rm g/m}V_{\rm g/m}/2e$ are the induced numbers of Cooper pairs on the gate and measurement capacitances respectively. We note that the quantum capacitance is positive in the ground state and negative in the excited state, as illustrated in figure 4. The absolute value is largest at the charge degeneracy $n_{\rm g} + n_{\rm m} = 0.5$

$$C_{\rm Q}^{\rm max} = \frac{C_{\rm m}^2}{C_\Sigma} \frac{E_{\rm Q}}{E_{\rm J}}. \tag{6}$$

The quantum capacitance can be an order of magnitude larger than the geometric capacitance for realistic parameters. By inserting the Cooper-pair box in a resonant LC-circuit and detecting its influence on the resonance frequency, the quantum capacitance was recently measured by two different groups [15, 16]. The measurement set-up is similar to the set-up that would be used for qubit read-out and is analysed below.

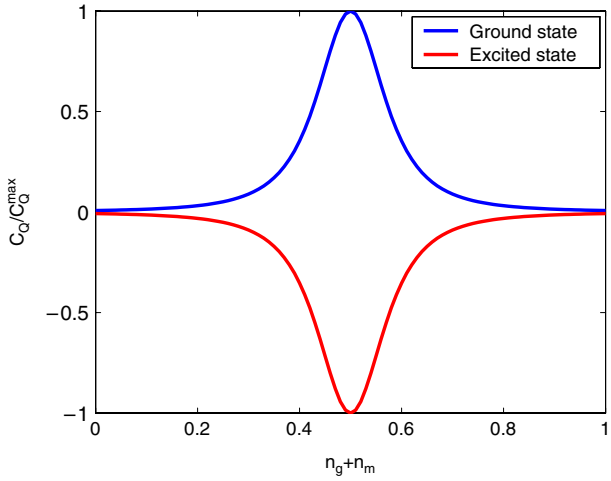

Figure 4. The quantum capacitance of a single-Cooper-pair box with $E_J/E_Q = 0.2$. Here normalized by the maximum value $C_Q^{max} = \frac{C_m^2}{C_\Sigma}\frac{E_Q}{E_J}$.

4.2. Read-out by measuring the quantum capacitance

At the charge degeneracy point the effective capacitance of the SCB in the ground and excited states differs by $2C_Q^{max}$. Imbedding the SCB in a resonant circuit as shown in figures 3(a) and (c) we can detect the corresponding change in the oscillator resonance frequency $\omega_0^{g/e} = 1/\sqrt{L(C \pm C_Q^{max})} = \omega_0(1 \mp C_Q^{max}/2C)$, where $\omega_0 = 1/\sqrt{LC}$ is the bare resonance frequency. The voltage reflection amplitude $\Gamma(\omega) = V_{out}(\omega)/V_d(\omega)$ seen from the driving side of the transmission line can for a high quality oscillator be written

$$\Gamma(\omega) = \frac{1 + 2iQ\frac{(\omega-\omega_0)}{\omega_0}}{1 - 2iQ\frac{(\omega-\omega_0)}{\omega_0}} = e^{i\varphi_r}, \qquad \text{where } \varphi_r = 2\arctan\left(\frac{2Q(\omega-\omega_0)}{\omega_0}\right), \tag{7}$$

up to a constant phase depending on the length of the transmission line. Here Q is the resonator's quality factor, which for the circuitry in figure 3(a) is determined by the characteristic impedance on the transmission line Z_0 through $Q = \omega_0 LC^2/C_c^2 Z_0$. Since there is no dissipation in the oscillator we have $|\Gamma(\omega)| = 1$. Driving the oscillator at the bare resonance frequency $\omega_d = \omega_0$ the phase-difference between the ground and excited states of the qubit will be

$$\delta\varphi_r = \varphi_r^g - \varphi_r^e = 4\arctan(QC_Q^{max}/C). \tag{8}$$

The phase-difference can be detected by measuring the reflected signal in-phase and quadrature components after mixing it with the drive.

5. A quantum description of the quantum capacitance readout

Above we described the quantum capacitance of the Cooper-pair box and its use for qubit read-out in a quasiclassical manner, treating the oscillator, transmission line, drive and detection classically. In order to address questions about the optimal read-out time, quantum back-action on the qubit and quantum efficiency of the read-out process we need a fully quantum description of the system. In this paper we do not have the space to go into details, which will be published

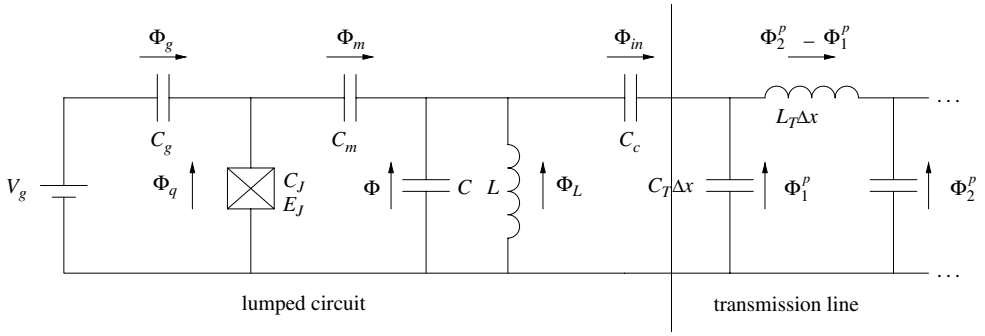

Figure 5. The circuit used for measurement of the quantum capacitance of the Cooper-pair box. It is similar to the circuit shown in figures 3(a) + (c), but the transmission line is here modelled as a semi-infinite line of LC-circuits in series. The phases $\Phi_i(t) = \int^t \mathrm{d}t'\, V_i(t')$ across the different circuit elements are the coordinates used in the Lagrangian describing the dynamics of the system.

elsewhere [48], but we will discuss the principles of our model and show a fully quantum derivation of the quantum capacitance.

The approach we chose is close to the 'quantum network theory' introduced by Yurke and Denker [49]. In section 5.1 we start by writing down the Lagrangian describing the classical dynamics of the circuit. Through a Legendre transform we arrive at the corresponding Hamiltonian. By stating canonical commutation relations between our phase coordinates Φ_i and their canonical conjugate momenta (charges) q_i

$$\left[\Phi_i, q_i\right] = \mathrm{i}\hbar \tag{9}$$

we arrive at a quantum Hamiltonian description of our circuit, which is discussed in section 5.2. In the relevant parameter regime we arrive at the expression for the quantum capacitance of the Cooper-pair box. Finally in section 5.3 we give an expression for the optimal qubit read-out time using homodyne detection.

5.1. Circuit Lagrangian

The circuit for performing read-out through the quantum capacitance is presented in figure 5. A Josephson charge qubit is capacitatively coupled to a harmonic oscillator, which is coupled to a transmission line. Through this line, all measurement on the qubit is performed. We model the line as a semi-infinite line of LC-circuits in series. The working point of the Josephson junction can be chosen using the bias V_g. In writing down the Lagrangian we are free to choose any quantities as our coordinates as long as they give a full description of our circuit. Since we are treating a system including a Josephson junction, the phases $\Phi_i(t) = \int^t \mathrm{d}t'\, V_i(t')$ across the circuit elements are natural coordinates, as discussed by Devoret in [50]. (This is in contrast to the original work by Yurke and Denker, where charges are chosen as coordinates.)

The capacitive energy of the circuit acts as the kinetic terms in the Lagrangian [3]

$$T = \tfrac{1}{2}\left(C_\mathrm{g}\dot{\Phi}_\mathrm{g}^2 + C_\mathrm{J}\dot{\Phi}_\mathrm{J}^2 + C_\mathrm{m}\dot{\Phi}_\mathrm{m}^2 + C\dot{\Phi}^2 + C_c\dot{\Phi}_{in}^2\right) + \tfrac{1}{2}\sum_{i=1}^{\infty}\Delta x C_T(\dot{\Phi}_i^p)^2 \tag{10}$$

and the inductive part plays the part of potential energy

$$V = \frac{\Phi_\mathrm{L}^2}{2L} - E_\mathrm{J}\cos\left(\frac{2e}{\hbar}\Phi_\mathrm{J}\right) + \sum_i \Delta x \frac{(\Phi_{i+1}^p - \Phi_i^p)^2}{2L_T(\Delta x)^2}. \tag{11}$$

Applying Kirchhoff's voltage law gives us the constraints

$$\begin{aligned} &\dot{\Phi}_{\mathrm{g}} - \dot{\Phi}_{\mathrm{J}} + V_{\mathrm{g}} = 0, \qquad &&\Phi_{\mathrm{J}} + \Phi_{\mathrm{m}} - \Phi = 0, \\ &\Phi_{in} + \Phi - \Phi_1^p = 0, \qquad &&\Phi - \Phi_{\mathrm{L}} = 0, \end{aligned} \tag{12}$$

which gives the Lagrangian for the system

$$\begin{aligned} L = {} & \frac{C_{\mathrm{qb}}\dot{\Phi}_{\mathrm{J}}^2}{2} + \frac{(C_{\mathrm{osc}} + C_c)\dot{\Phi}^2}{2} + \frac{C_c(\dot{\Phi}_1^p)^2}{2} - \frac{\Phi^2}{2L} + E_{\mathrm{J}}\cos\left(\frac{2e}{\hbar}\Phi_{\mathrm{J}}\right) \\ & - \frac{C_{\mathrm{m}}}{2}\dot{\Phi}\dot{\Phi}_{\mathrm{J}} - \frac{C_c}{2}\dot{\Phi}\dot{\Phi}_1^p - C_{\mathrm{g}}V_{\mathrm{g}}\dot{\Phi}_{\mathrm{J}} \\ & + \sum_{i=1}^{\infty}\Delta x\left(\frac{C_T(\dot{\Phi}_i^p)^2}{2} - \frac{(\Phi_{i+1}^p - \Phi_i^p)^2}{2L_T(\Delta x)^2}\right). \end{aligned} \tag{13}$$

The capacitances in the Lagrangian are now $C_{\mathrm{qb}} = C_{\mathrm{J}} + C_{\mathrm{g}} + C_{\mathrm{m}}$, and $C_{\mathrm{osc}} = C + C_{\mathrm{m}}$.

5.2. Hamiltonian and quantum capacitance

From the Lagrangian we easily obtain the Hamiltonian through a Legendre transform. We present the Hamiltonian in the form

$$H = H_{\mathrm{qb}} + H_{\mathrm{osc}} + H_{\mathrm{TL}} + H_{\mathrm{int}}, \tag{14}$$

and for simplicity we assume weak coupling $C_{\mathrm{m}} \ll \{C_{\mathrm{osc}}, C_{\mathrm{qb}}\}$ and present only the lowest order (in $C_{\mathrm{m}}/\{C_{\mathrm{qb}}, C_{\mathrm{osc}}\}$) terms. H_{qb} contains the qubit degrees of freedom including the coupling of the qubit to the rest of the system

$$H_{\mathrm{qb}} = \frac{1}{2C_{\mathrm{qb}}}(q_{\mathrm{J}} + C_{\mathrm{g}}V_{\mathrm{g}})^2 + \frac{C_{\mathrm{m}}}{C_{\mathrm{qb}}C_{\mathrm{osc}}}\left(q + q_p\right)(q_{\mathrm{J}} + C_{\mathrm{g}}V_{\mathrm{g}}) - E_{\mathrm{J}}\cos\left(\frac{2e}{\hbar}\Phi_{\mathrm{J}}\right), \tag{15}$$

while the terms describing the oscillator, transmission line and their interaction are

$$\begin{aligned} &H_{\mathrm{osc}} = \frac{q^2}{2C_{\mathrm{osc}}} + \frac{\Phi^2}{2L}, \qquad H_{\mathrm{TL}} = \frac{q_p^2}{2C_c} + \frac{1}{\Delta x}\sum_{i=1}^{\infty}\left(\frac{(q_{(i+1)}^p)^2}{2C_T} + \frac{(\Phi_{i+1}^p - \Phi_i^p)^2}{2L_T}\right), \\ &H_{\mathrm{int}} = \frac{qq_p}{C_{\mathrm{osc}}}, \end{aligned} \tag{16}$$

where the charge operators q, q_{J}, q_p and q_i^p are the conjugate momenta to phase operators Φ, Φ_{J}, Φ_1^p and Φ_i^p respectively. For realizing a charge qubit the box charging energy $E_{\mathrm{C}} = e^2/2C_{\mathrm{qb}}$ is much smaller than the Josephson energy $E_{\mathrm{C}} \gg E_{\mathrm{J}}$. For relevant parameters we can then limit the qubit charge q_{J} to the two values $\{0, 2\}$e, and we get the usual expression for the qubit Hamiltonian in the language of the Pauli spin matrices

$$H_{\mathrm{qb}} = -\frac{E_{\mathrm{el}}}{2}\sigma_z - \frac{E_{\mathrm{J}}}{2}\sigma_x + 2E_{\mathrm{C}}\kappa\frac{q + q_p}{e}\sigma_z + 2E_{\mathrm{C}}\kappa\frac{q + q_p}{e}(1 - n_0), \tag{17}$$

where we introduce the electrostatic energy-difference of the qubit states $E_{\mathrm{el}} = 4E_{\mathrm{C}}(1 - n_0)$, the dimensionless charge $n_0 = C_{\mathrm{g}}V_{\mathrm{g}}/e$, and the oscillator-qubit coupling coefficient $\kappa = C_{\mathrm{m}}/C_{\mathrm{osc}} \ll 1$. The last term does not influence the system dynamics and may be absorbed in a small shift of q and q_p. Rotating the remaining two terms to the eigenbasis of the qubit

$$H_{\mathrm{qb}} = \sigma_z\sqrt{16E_{\mathrm{C}}^2\left(1 - n_0 - \kappa(q + q_p)/e\right)^2 + E_{\mathrm{J}}^2/4}, \tag{18}$$

we arrive at the usual charge qubit Hamiltonian with the charge induced by the oscillator added to the induced gate charge. We now concentrate on the case when the oscillator frequency $\omega_0 = 1/\sqrt{LC_{\mathrm{osc}}}$ is much lower than qubit frequency $E_{\mathrm{J}}/\hbar$. Furthermore, we consider the

amplitude of the oscillator charge oscillations q_0 such that the induced charge oscillations in the qubit are small, $\kappa q_0/e \ll E_J/4E_C \ll 1$. In this case the qubit will follow the oscillator dynamics adiabatically and the rates for transition between the qubit eigenstates are negligible. Furthermore, we may Taylor expand the qubit energy around the working point and at the charge degeneracy $n_0 = 1$ we arrive at the final Hamiltonian

$$H = -\frac{E_J}{2}\sigma_z + \left(\frac{1}{2C_{osc}} + \frac{4\kappa^2 E_C^2}{e^2 E_J}\sigma_z\right)(q+q_p)^2 + \frac{\Phi^2}{2L} + \frac{q_p^2}{2C_c} + \frac{1}{\Delta x}\sum_{i=1}^{\infty}\left(\frac{(q_{i+1}^p)^2}{2C_T} + \frac{(\Phi_{i+1}^p - \Phi_i^p)^2}{2L_T}\right). \tag{19}$$

The qubit thus shifts the capacitative energy of the oscillator, which in turn corresponds to adding a small extra capacitor to the oscillator $C_\Sigma = C_{osc} + C_Q$, where the *quantum capacitance* C_Q is given by

$$C_Q = -\frac{2e^2 C_m^2}{E_J C_{qb}^2}\sigma_z, \tag{20}$$

which is identical to the semiclassical formula in equation (6). This in turn will shift the resonance frequency of the oscillator by an amount $\delta\omega = -\sigma_z\omega_0 C_Q/2C_{osc}$.

5.3. Qubit read-out using homodyne detection

Taking the continuum limit $\Delta x \to 0$ in equation (19) the solutions to the Hamiltonian for the transmission line correspond to fields $\Phi(x \pm vt)$ propagating to the left and right with velocity $v = 1/\sqrt{C_T L_T}$. From the Hamiltonian we derive equations of motion from which the right-propagating out-field $\Phi^{out}(t)$ and the charge on the oscillator $q(t)$ can expressed in terms of the left-propagating in-fields $\Phi^{in}(t)$, which is determined by the drive. In the parameter regime relevant for qubit read-out, where the amplitude of the qubit charge oscillations induced by the LC-circuit is small, the qubit will follow the oscillator adiabatically. Furthermore it is adequate to neglect third and higher order terms in the Taylor expansion of the qubit energy in equation (18). Thus we arrive at linear equations of motion which we may solve in Fourier representation

$$\begin{aligned}
&\chi(\omega) = \frac{\mathrm{i}2C_c C_\Sigma L\omega^3}{1-(C_\Sigma + C_c)L\omega^2 - \mathrm{i}\omega C_c Z_0(1 - LC_\Sigma\omega^2)},\\
&q(\omega) + q_p(\omega) = \chi(\omega)\Phi_p^{in}(\omega),\\
&\Phi^{out}(\omega) = \frac{\chi(\omega)}{\chi^*(\omega)}\Phi_p^{in}(\omega) = S(\omega)\Phi_p^{in}(\omega),
\end{aligned} \tag{21}$$

where $Z_0 = \sqrt{L_T/C_T}$ is the characteristic impedance of the transmission line. Since there is no dissipation in the lumped circuit we have $|\Phi^{out}(\omega)| = |\Phi^{in}(\omega)|$. In this linear regime the Heisenberg equations of motion are similar to the classical ones, and for a high quality oscillator we have $S(\omega) = \Gamma(\omega)$ as given in equation (7). To discuss the quantum statistics of the qubit read-out we need a quantized representation of the fields

$$\begin{aligned}
\Phi^{in}(t) &= \sqrt{\frac{\hbar Z_0}{4\pi}}\int_0^\infty \frac{\mathrm{d}\omega}{\sqrt{\omega}}\left[a_\omega^{in}\mathrm{e}^{-\mathrm{i}\omega t} + (a_\omega^{in})^\dagger \mathrm{e}^{\mathrm{i}\omega t}\right],\\
\Phi^{out}(t) &= \sqrt{\frac{\hbar Z_0}{4\pi}}\int_0^\infty \frac{\mathrm{d}\omega}{\sqrt{\omega}}\left[S(\omega)a_\omega^{in}\mathrm{e}^{-\mathrm{i}\omega t} + S(\omega)^*(a_\omega^{in})^\dagger \mathrm{e}^{\mathrm{i}\omega t}\right],\\
q(t) &= \sqrt{\frac{\hbar Z_0}{4\pi}}\int_0^\infty \frac{\mathrm{d}\omega}{\sqrt{\omega}}\left[\chi(\omega)a_\omega^{in}\mathrm{e}^{-\mathrm{i}\omega t} + \chi(\omega)^*(a_\omega^{in})^\dagger \mathrm{e}^{\mathrm{i}\omega t}\right],
\end{aligned} \tag{22}$$

where the in-field annihilation and creation operators obey the canonical commutation relations

$$[a_\omega, a^\dagger_{\omega'}] = \delta(\omega - \omega'), \qquad \text{and} \qquad [a_\omega, a_{\omega'}] = 0. \tag{23}$$

What we have achieved is a complete quantum description of the dynamics of the oscillator and qubit in terms of the incident field from the transmission line. We also get a full description of the outgoing field, which is what will enter the detector. The linearity of the equations of motion arises since we have approximated the qubit with a state-dependent capacitance. This is valid as long as the amplitudes of the charge oscillations induced on the qubit island are small, so that a second order Taylor expansion of the energy in equation (18) is enough. Furthermore, we neglect transitions between the qubit states, which can be done for small amplitude oscillations and a low oscillator frequency $\hbar\omega_0 \ll E_\mathrm{J}$.

We now have the formalism needed to address questions about the readout time, which we do in the next section. We can also calculate the back-action of the measurement process on the qubit. This and the issue of the quantum efficiency, i.e. the relation between the qubit dephasing rate and the measurement time, will be addressed elsewhere [48].

By measuring the power of the reflected signal mixed with a local oscillator, e.g. the drive itself, and then a local oscillator shifted by 90°, the in-phase and quadrature signal amplitude can be extracted, as was done in [25]. For optimized qubit read-out it is advantageous to implement the standard quantum optics scheme of homodyne detection [52].

To model a measurement we thus put the in-field in a coherent Glauber state [51]

$$|\{\alpha(\omega)\}\rangle = \exp\left(\int \mathrm{d}\omega\, [\alpha(\omega)(a^{\mathrm{in}}_\omega)^\dagger - \alpha^*(\omega) a^{\mathrm{in}}_\omega]\right)|0\rangle, \tag{24}$$

where $\alpha(\omega)$ is the Fourier-transform of our drive signal, and $|0\rangle$ is the continuum vacuum field $a_\omega|0\rangle = 0$. We model our drive source with a narrow ($\Gamma_\mathrm{d} \ll \omega_\mathrm{d}$) Gaussian distribution in frequency

$$\alpha(\omega) = \alpha_0 \frac{\omega_\mathrm{d}}{\Gamma_\mathrm{d}} \frac{\mathrm{e}^{-(\omega-\omega_\mathrm{d})^2/2\Gamma_\mathrm{d}^2}}{\sqrt{\omega}}, \tag{25}$$

where α_0 is a dimensionless constant. For $|t| \ll \Gamma_\mathrm{d}^{-1}$ this gives the average electrical field

$$\bar{V}^{\mathrm{in}}(x,t) = -\alpha_0\sqrt{2\hbar Z_0}\omega_\mathrm{d} \sin\left[\omega_\mathrm{d}(t + x/v)\right], \tag{26}$$

giving on average $\Gamma^{\mathrm{in}}_n = \alpha_0^2\omega_\mathrm{d}$ photons per second sent through the transmission line by the drive.

The annihilation operator for the reflected signal has the amplitude $a^{\mathrm{out}}_\omega = S(\omega)a^{\mathrm{in}}_\omega \approx \mathrm{e}^{-(\omega_\mathrm{d}t - \varphi_r^{\mathrm{g/e}})}a^{\mathrm{in}}_\omega$ depending on the qubit state. The signal is mixed with a strong local oscillator with amplitude $\alpha_\mathrm{LO}\mathrm{e}^{-(\omega_\mathrm{d}t-\varphi_\mathrm{LO})}$ and the intensity is detected. The result is then integrated for a time T. The intensity is given by the number of photons incident on the detector

$$N(\omega, T) = \int_0^T \mathrm{d}t\, b^\dagger(t) b(t) \tag{27}$$

where the field at the detector is

$$b(t) = r\alpha_\mathrm{LO}(t) + rv(t) + ta^{\mathrm{out}}(t); \tag{28}$$

here $r \ll 1$ denotes the small reflection coefficient of the mixer and t is the corresponding transmission coefficient, and $v(t)$ is the vacuum field of the idle mixer port. (The mixer is a beam-splitter in the quantum optics case.) We now assume that $|r\alpha_\mathrm{LO}(t)| \gg 1$ is large and neglect second order contributions in $v(t)$ and $a(t)$ to equation (27), arriving at the average photon number at the detector

$$\langle N^{\mathrm{g/e}}\rangle = T\left(r^2\alpha^2_\mathrm{LO} + 2tr\alpha_\mathrm{LO}\alpha_0^{\mathrm{in}}\cos\left(\varphi_r^{\mathrm{g/e}} - \varphi_\mathrm{LO}\right)\right), \tag{29}$$

where $\alpha_0^{\rm in}$ is the amplitude of the in-field. The first term is a pure local oscillator term and contains no information, while the second term is maximized choosing $\varphi_{\rm LO} = \frac{\varphi_r^g + \varphi_r^e}{2} - \frac{\pi}{2}$. The two probability distributions of the number of detected photons will be separated by twice the variance after the measurement time

$$T_{\rm ms} = \frac{1}{\Gamma_n^{\rm in}} \frac{1}{4\sin^2\left[\frac{\varphi_r^g - \varphi_r^e}{2}\right]}, \tag{30}$$

where $\Gamma_n^{\rm in}$ is rate of photons sent into the transmission line by the drive. For not too low quality factor of the oscillator we can use the Breit–Wigner approximation for $\chi(\omega)$ leading to the expression for the phase-shift in equation (8). Thus we find for the measurement time

$$T_{\rm ms} = \frac{1}{\Gamma_n^{\rm in}} \frac{1}{4\sin^2\left[2\arctan x\right]} = \frac{(x^{-1} + x)^2}{16\Gamma_n^{\rm in}}, \qquad x = \frac{QC_{\rm Q}^{\rm max}}{C}. \tag{31}$$

From the condition that the drive should induce only small oscillations of the qubit charge we arrive at the following bound for the drive strength:

$$\Gamma_n^{\rm in} < \frac{E_{\rm J}}{16\hbar}(x + x^{-1}) \tag{32}$$

giving a lower bound on measurement time

$$T_{\rm ms} > \frac{\hbar}{E_{\rm J}}(x + x^{-1}), \tag{33}$$

indicating that the measurement time must be larger than $\hbar/E_{\rm J}$, which is not very restrictive. Due to the oscillator 'ring-up' time the measurement time is further limited by $T_{\rm ms} > Q/\omega_0 = xC/C_{\rm Q}\omega_0$. For a fixed ω_0 this indicates that the regime $x \ll 1$ is advantageous. Comparing these two inequalities we find the shortest measurement time for

$$x_{\rm opt}^2 = \frac{C_{\rm Q}}{C}\frac{\hbar\omega_0}{E_{\rm J}}, \qquad Q_{\rm opt} = \sqrt{\frac{C}{C_{\rm Q}}\frac{\hbar\omega_0}{E_{\rm J}}}, \qquad \text{and} \qquad T_{\rm ms} > \frac{Q_{\rm opt}}{\omega_0}, \tag{34}$$

implying that a low Q is clearly an interesting regime. For low Q the Breit–Wigner approximation of $\chi(\omega)$ breaks down, and so does the simple estimate of the measurement, but the formalism developed here is still applicable using the full expressions. An optimization including the measurement induced back-action on the qubit will be discussed in [48].

5.4. A comparison with dispersive readout using a non-adiabatic oscillator

In an experiment at Yale University [53] a charge qubit coupled capacitatively to a microstrip cavity was read out by sending microwaves through the cavity. The qubit state influences the resonance frequency and thus the phase-shift of the transmitted signal. This phase difference was then detected in a similar fashion as described above.

The main difference compared to what was discussed above is that the cavity resonance frequency (5.4 GHz) was of the same order of magnitude as the qubit frequency (4.3 GHz). In this regime it is appropriate to use the rotating wave approximation and the system dynamics is described by the Jaynes–Cummings Hamiltonian [10].

For a comparison we start with the Hamiltonian of a qubit coupled transversely to a harmonic oscillator

$$H = -\frac{\hbar\omega_{\rm qb}}{2}\sigma_z + {\rm i}g\sigma_x(a^\dagger - a) + \hbar\omega_{\rm osc}\left(a^\dagger a + \frac{1}{2}\right), \tag{35}$$

applicable for a charge qubit at charge degeneracy, coupled capacitatively to the harmonic oscillator. Performing a straightforward second order perturbation expansion in the coupling term we find the renormalized spectrum

$$E_{n\uparrow} = \hbar\omega_{\rm osc}\left(n+\frac{1}{2}\right) - \frac{\hbar\omega_{\rm qb}}{2} - g^2\left[\frac{n}{\hbar\omega_{\rm qb}-\hbar\omega_{\rm osc}} + \frac{n+1}{\hbar\omega_{\rm qb}+\hbar\omega_{\rm osc}}\right] \quad \text{and}$$
$$E_{n\downarrow} = \hbar\omega_{\rm osc}\left(n+\frac{1}{2}\right) + \frac{\hbar\omega_{\rm qb}}{2} + g^2\left[\frac{n}{\hbar\omega_{\rm qb}+\hbar\omega_{\rm osc}} + \frac{n+1}{\hbar\omega_{\rm qb}-\hbar\omega_{\rm osc}}\right], \tag{36}$$

where n indicates the number of photons in the oscillator and $\uparrow/\downarrow$ the qubit in the ground/excited state for the unperturbed state ($g \to 0$). The spectrum is formed by two equidistant sets of energy levels, where the effective qubit-dependent frequency shift of the oscillator amounts to

$$\delta\omega = -\sigma_z g^2\left[\frac{1}{\hbar\omega_{\rm qb}-\hbar\omega_{\rm osc}} + \frac{1}{\hbar\omega_{\rm qb}+\hbar\omega_{\rm osc}}\right], \tag{37}$$

being negative for the qubit in the ground state. In the regime $|\omega_{\rm qb}-\omega_{\rm osc}| \ll \omega_{\rm qb}$ only the first term contributes and we arrive at the Jaynes–Cummings result $\delta\omega = -\sigma_z g^2/(\hbar\omega_{\rm qb}-\hbar\omega_{\rm osc})$. In the adiabatic regime $\omega_{\rm osc} \ll \omega_{\rm qb}$ we can neglect the terms $\pm\hbar\omega_{\rm osc}$ in the denominators, giving the result below equation (20), $\delta\omega = -\sigma_z 2g^2/\hbar\omega_{\rm qb}$. Thus we see that the frequency shift given by the Jaynes–Cummings Hamiltonian can be described on the same footing as the one given by the quantum capacitance.

6. Flux measurement

The two-level quantum states of the persistent-current flux qubit (figure 1) are characterized by different directions of the persistent currents circulating in the qubit loop, hence different directions of the induced magnetic flux. The flux qubit readout is based on the detection of the induced flux or direct measurement of the persistent currents. The latter method is also relevant for charge qubits with loop-shape electrodes (e.g. quantronium [28]), where the intensity of the induced flux is too small to be detectable while detection of the persistent current is possible. In flux qubits with larger Josephson junctions, persistent currents are large, and the measurement of flux is not that difficult [18, 20, 35, 55]. The experimental measurement set-up is sketched in figure 1, left picture: the qubit loop is inductively coupled to a dc-SQUID connected to a current source. The direction of the persistent current in the qubit loop affects the magnetic flux threading the SQUID and thus affects the SQUID critical current as well as its plasma frequency. This allows one to make the two types of measurements, by probing the dc and the ac properties of the measurement SQUID. In the first case, the critical current is measured by applying a dc current slowly increasing with time, and detecting the value of the critical current when the SQUID switches to the resistive branch (threshold detection), repeating the measurement to create a histogram of the events. In the second case, an ac current is applied and the phase shift of the reflected signal is measured. The latter method is also possible to realize using a linear LC-oscillator instead of the dc SQUID [18].

To quantitatively analyse the circuit (see e.g. [3, 21, 54]), let us for simplicity consider the single-junction flux qubit; the analysis also applies to the experimental three-junction qubits. The circuit Hamiltonian consists of the Hamiltonian $H_{\rm q}$ of the qubit loop, the Hamiltonian of the SQUID, $H_{\rm S}$, and the Hamiltonian of the inductive coupling, $H_{\rm int}$. The qubit Hamiltonian has the form given in equation (2); here, we modify the notations,

$$H_{\rm q} = E_{Cq} n_{\rm q}^2 - E_{Jq}\cos\phi_{\rm q} + E_{Lq}\tilde{\phi}_{\rm q}^2, \tag{38}$$

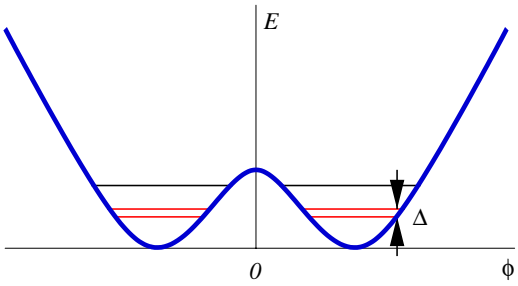

Figure 6. Double-well potential and energy levels of the flux qubit ($f_q = \pi$).

where $E_{Cq} = (2e)^2/2C_q$ is the charging energy of the qubit junction, E_{Jq} is the Josephson energy, $E_{Lq} = (\Phi_0/2\pi)^2(1/2L_q)$ is the inductive energy of the qubit loop, and $\tilde{\phi}_q = \phi_q - f_q$ is the induced flux; f_q is the biasing flux. The SQUID Hamiltonian is given by

$$H_s = \sum_i^2 (E_{Cs} n_i^2 - E_{Js} \cos\phi_i) + E_{Ls}\phi_s^2 + \frac{\hbar}{4e} I(t)(\phi_1 - \phi_2), \tag{39}$$

where the induced flux is $\phi_s = \phi_1 + \phi_2 - f_s$, and $I(t)$ is a (non)stationary current bias. The interaction term has the form

$$H_{int} = E_M \tilde{\phi}_q \phi_s, \tag{40}$$

where the interaction energy is determined by the mutual inductance M, $E_M = (\Phi_0/2\pi)^2(M/L_qL_s)$.

Now we truncate the Hilbert space of the circuit Hamiltonian to the lowest energy states, which include the two almost degenerate (for $E_{Cq} \ll E_{Jq}$ and at $f_q \approx \pi$) lowest energy states in the potential wells of the qubit potential energy, figure 6, and the ground state of the SQUID. Then the qubit Hamiltonian takes the form, in the eigenbasis of the non-coupled wells,

$$H_q = -\tfrac{1}{2}(\epsilon\sigma_z + \Delta\sigma_x). \tag{41}$$

Here $\epsilon(f_q)$ is the energy level difference in the wells proportional to $f_q - \pi$, and Δ is the energy level splitting due to the macroscopic tunnelling between the wells. The truncated interaction term takes the form

$$H_{int} = E_M \phi_0 \phi_s \sigma_z, \tag{42}$$

where ϕ_0 is the half distance between the minima of the potential energy. The off-diagonal term in the interaction is neglected since it is exponentially small.

To truncate the SQUID Hamiltonian, we introduce new variables, $\phi_\pm = (1/2)(\phi_1 \pm \phi_2)$, and $\phi_s = 2\phi_+ - f_s$,

$$H_s = \frac{1}{2}E_{Cs}n_-^2 + 2E_{Cs}n_s^2 - 2E_{Js}\cos\phi_- \cos\left(\frac{f_s + \phi_s}{2}\right) + E_{Ls}\phi_s^2 + \frac{\hbar}{2e}I(t)\phi_-. \tag{43}$$

Now we assume that the inductive energy is sufficiently large, $E_{Ls} \gg E_{Js}$, to provide small fluctuation of the induced flux, $\phi_s \ll 1$. This allows us to expand the cosine term; then keeping the first order term with respect to ϕ_s (non-vanishing for $f_s \neq 0$), and taking into account the interaction term (42), we write the ϕ_s-dependent part of the total Hamiltonian in the form

$$H(\phi_s) = 2E_{Cs}n_s^2 + \left(E_{Js}\cos\phi_- \sin\left(\frac{f_s}{2}\right) + E_M\phi_0(f_q)\sigma_z\right)\phi_s + E_{Ls}\phi_s^2. \tag{44}$$

This is the linear oscillator shifted from the origin, the shift being proportional to the induced flux in the qubit loop. Making a projection on the ground state of this Hamiltonian, we arrive at the non-trivial, qubit-dependent part having the form

$$H(\phi_s) \to -2E_{Js}\lambda \sin\left(\frac{f_s}{2}\right)\sigma_z \cos\phi_-, \qquad \lambda = \frac{E_M\phi_0}{8E_{Ls}}. \tag{45}$$

Combining this with the rest of the SQUID Hamiltonian and the truncated qubit Hamiltonian, we finally get

$$H = -\frac{1}{2}(\epsilon\sigma_z + \Delta\sigma_x) + \frac{1}{2}E_{Cs}n_-^2 - 2E_{Js}\left[\cos\left(\frac{f_s}{2}\right) + \lambda\sin\left(\frac{f_s}{2}\right)\sigma_z\right]\cos\phi_- + \frac{\hbar}{2e}I(t)\phi_-. \tag{46}$$

For the three-junction qubit [32] the coupling constant λ in equation (45) acquires an additional factor [56] E_{Jq}/E_{Lq}, which results from tracing out the plasma mode in the qubit loop. This mode does not form the qubit in the three-junction circuit (in contrast to the single-junction qubit), but this mode is an auxiliary one connecting the qubit to the outside world, and it is eliminated similarly to the SQUID variable ϕ_+ in equations (44) and (45).

The Hamiltonian (46) describes a flux qubit directly coupled via an effective coupling constant λ to a non-linear Josephson oscillator. The coupling affects the Josephson energy of the oscillator, hence the critical bias current, i.e. the the magnitude of the bias dc current at which the oscillator switches to the dissipative regime. Quantitatively, these critical current values for the three-junction qubit are

$$\frac{\hbar}{2e}I_c = 2E_{Js}\left(\cos(f_s/2) \pm \lambda\frac{E_{Jq}}{E_{Lq}}\sin(f_s/2)\right). \tag{47}$$

The advantage of this method is that the measurement circuit can be disconnected during the time period between the measurements by switching off the flux through the SQUID, $f_s = 0$, thus enhancing the decoherence time of the qubit. The disadvantage of the method is that for slow readout (low Josephson plasma frequency of the SQUID compared to the qubit frequency) the switching current depends on the average value of the induced flux, $\langle\sigma_z\rangle$, which equals zero at the degeneracy point, $\epsilon = 0$. Thus measurement can only be performed by departing from the degeneracy point, which is undesirable due to enhanced decoherence. This difficulty can be solved by probing the qubit quantum inductance, which is analogous to the quantum capacitance measurement for charge qubits.

7. Inductance measurement

Consider first a simpler circuit with a linear LC-oscillator replacing the dc SQUID (figure 7). Such a device, an rf-SQUID inductively coupled to a linear oscillator, is a classical device employed for many years for precise measurement of magnetic field [57]. The principle of operation is based on the magnetic field dependence of the Josephson inductance, which affects the resonance frequency of the oscillator probed by an external rf signal. The classical Hamiltonian for this circuit, again assuming for simplicity a single Josephson junction in the qubit loop, has the form

$$H = E_{Cq}n_q^2 - E_{Jq}\cos\phi_q + E_{Lq}\tilde{\phi}_q^2 + E_M\tilde{\phi}_q\phi + E_{Cosc}n^2 + E_{Losc}\phi^2 + \frac{\hbar}{2e}I(t)\phi. \tag{48}$$

Neglecting the junction capacitance energy, and expanding the qubit potential energy near the minimum point $\tilde{\phi}_{q0}(f_q)$,

$$-E_{Jq}\cos\phi_q + E_{Lq}\tilde{\phi}_q^2 \equiv U(\tilde{\phi}_q) = U(\tilde{\phi}_{q0}) + \tfrac{1}{2}U''(\tilde{\phi}_{q0})(\tilde{\phi}_q - \tilde{\phi}_{q0})^2, \tag{49}$$

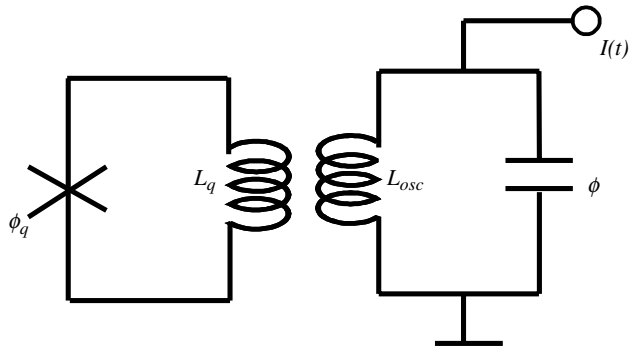

Figure 7. Single-contact flux qubit inductively coupled to a linear oscillator.

we define an effective inductance of the qubit circuit $L_{\rm q}^{\rm eff}$ via the relation

$$\tfrac{1}{2}U''(\tilde{\phi}_{\rm q0}) = (\Phi_0/2\pi)^2/2L_{\rm q}^{\rm eff}(f_{\rm q}) = E_{{\rm L}q}^{\rm eff}(f_{\rm q}). \tag{50}$$

After having diagonalized the total potential energy, we obtain the shift of the oscillator inductive energy due to coupling to the qubit,

$$\tilde{E}_{\rm Losc} = E_{\rm Losc} - \frac{E_M^2}{4E_{{\rm L}q}^{\rm eff}(f_{\rm q})}. \tag{51}$$

This gives rise to a shift of the oscillator resonance frequency depending on the magnetic flux through the qubit loop, which is probed with an external rf signal $I(t)$.

A similar measurement procedure also applies to the quantum regime. The quantum Hamiltonian for the same circuit has the form, taking into account equations (41) and (42),

$$H = -\frac{1}{2}(\epsilon\sigma_z + \Delta\sigma_x) + E_M\phi_0\phi\sigma_z + E_{\rm Cosc}n^2 + E_{\rm Losc}\phi^2 + \frac{\hbar}{2e}I(t)\phi. \tag{52}$$

For a slow oscillator and weak coupling, the Hamiltonian can be rotated to a qubit eigenbasis, and expanded with respect to the coupling term,

$$H = -\frac{1}{2}\varepsilon\sigma_z - \frac{(E_M\phi_0)^2}{\varepsilon}\phi^2\sigma_z + E_{\rm Cosc}n^2 + E_{\rm Losc}\phi^2 + \frac{\hbar}{2e}I(t)\phi \tag{53}$$

(here the term linear in ϕ is omitted since it only produces a non-essential small shift of the oscillator coordinate; $\varepsilon = \sqrt{\epsilon^2 + \Delta^2}$). The second term in equation (53) provides the shift of the oscillator inductive energy depending on the qubit state,

$$\tilde{E}_{\rm Losc} = E_{\rm Losc} - \frac{E_M^2\phi_0^2}{\varepsilon}\sigma_z. \tag{54}$$

Comparing this quantum result with the classical equation (51), we are able to identify the quantum inductance of the qubit,

$$L_{\rm Q} = \left(\frac{2\pi}{\Phi_0}\right)^2 \frac{2\phi_0^2}{\varepsilon}\sigma_z. \tag{55}$$

The quantum inductance is inversely proportional to the qubit level splitting, similar to the quantum capacitance of charge qubits, and it approaches its maximum value at the degeneracy point.

This conclusion also applies to the three-junction flux qubit [32]; the only difference is due to the suppressed coupling of the qubit to the outside world discussed in the previous section

below equation (46). In this case, an additional small factor, E_{Jq}/E_{Lq}, appears in the coupling term in equation (52), giving rise to the following equation for the quantum inductance of the three-junction qubit:

$$L_Q = \left(\frac{2\pi}{\Phi_0}\right)^2 \left(\frac{E_{Jq}}{E_{Lq}}\right)^2 \frac{2\phi_0^2}{\varepsilon}\sigma_z. \tag{56}$$

Proceeding with the case of the readout dc SQUID, equation (46), we find that this case seems to be qualitatively different from the LC-oscillator readout: the qubit–meter coupling is non-linear. Obviously, this results from the fact that the qubit is not directly coupled to the readout ϕ_--oscillator, but rather via an intermediate ϕ_s-oscillator, the elimination of which results in the non-linear coupling.

One way to solve the problem is to displace the ϕ_--oscillator by applying a constant current bias, $I(t) = I_0 + I_1(t)$. Then expanding the potential energy around the minimum point, $\phi_- = \bar{\phi}_- + \theta$, where $\bar{\phi}_-$ satisfies the equation $2E_{Js}\cos(f_s/2)\sin\bar{\phi}_- = -(\hbar/2e)I_0$, we arrive, in the linear approximation, at a Hamiltonian similar to equation (52),

$$H = -\frac{1}{2}(\epsilon\sigma_z + \Delta\sigma_x) + \frac{1}{2}E_{Cs}n_-^2 + E_{Js}\cos\bar{\phi}_-\cos(f_s/2)\theta^2 + \tilde{\lambda}E_{Js}\theta\sigma_z + \frac{\hbar}{2e}I_1(t)\theta, \tag{57}$$

$$\tilde{\lambda} = \lambda\frac{\hbar I_0 E_{Jq}}{2eE_{Lq}}\tan(f_s/2)\,. \tag{58}$$

Another solution would be to access directly the ϕ_s-oscillator linearly coupled to the qubit. This can be done, for example, by driving a bias flux through the SQUID, $f_s(t)$. For small variation of phases in equation (43), the oscillators decouple, and the relevant part of the Hamiltonian, taking into account equations (41) and (42), approaches a form similar to equation (52),

$$H = -\frac{1}{2}(\epsilon\sigma_z + \Delta\sigma_x) + 2E_{Cs}n_s^2 + E_{Js}\phi_s^2 + \frac{E_M E_{Jq}\phi_0}{E_{Lq}}\phi_s\sigma_z + 2E_{Js}f_s(t)\phi_s. \tag{59}$$

Finally, the ϕ_s-oscillator may be accessed by using an asymmetric SQUID, with different inductances of the left and right legs (figure 1), $L_1 \neq L_2$, $L_1 + L_2 = L_s$. In this case, the coupling of the SQUID to an external current source in equation (39) becomes modified to

$$\frac{\hbar}{4e}I(t)\left(\frac{L_2}{L_s}\phi_1 - \frac{L_1}{L_s}\phi_2\right), \tag{60}$$

which results in direct coupling of the probing current to the ϕ_s-oscillator. At zero flux bias, $f_s = 0$, the two $\phi_\pm$-oscillators do not interact, and the relevant part of the Hamiltonian reads

$$H = -\frac{1}{2}(\epsilon\sigma_z + \Delta\sigma_x) + 2E_{Cs}n_s^2 + (E_{Ls} + E_{Js})\phi_s^2 + \frac{E_M E_{Jq}\phi_0}{E_{Lq}}\phi_s\sigma_z + \frac{\hbar}{2e}I(t)\frac{L_2 - L_1}{L_s}\phi_s. \tag{61}$$

Thus there are several ways to employ the dc SQUID for dispersive measurement of the qubit quantum inductance. Note, however, that in the latter case the inductive energy of the SQUID plays a role, and for small SQUID inductance ($E_{Ls} \gg E_{Js}$) the oscillator frequency may become large, violating the adiabatic regime assumed in the derivation.

8. Concluding remarks

In this paper we have outlined some practical schemes for capacitive and inductive readout, detecting the state of a qubit by reflecting microwaves from an oscillator circuit, the phase shift measuring the changes in charge or magnetic flux induced by a qubit, allowing us to distinguish between the different states $|0\rangle$ and $|1\rangle$ of the qubit. In particular, we focused attention on

the single-Cooper-pair box (SCB), the effective capacitance of which can be defined as the derivative of the induced charge with respect to gate voltage. In addition to the geometric capacitance, there is the quantum capacitance due to the level dispersion at the anti-crossing caused by the Josephson coupling. We described the process of reflection of quantized radiation and derived expressions for the shortest measurement time needed to resolve the qubit states, suggesting that a low Q should be advantageous for weak back-action fast readout.

Acknowledgment

This work was supported in part by the European Commission through projects FP5-39083-SQUBIT-2 and FP6-015708 EuroSQIP of the IST Priority (disclaimer www.eurosqip.org), and by the Swedish Research Council.

References

[1] Esteve D and Vion D 2004 Solid state quantum bit circuits *Les Houches Summer School-Session LXXXI on Nanoscopic Quantum Physics*

[2] Elzerman J M, Hanson R, Willems van Beveren L H, Witkamp B, Greidanus J S, Schouten R N, De Franceschi S, Tarucha S, Vandersypen L M K and Kouwenhoven L P 2005 Semiconductore few-electron quantum dots as spin qubits *Quantum Dots: A Doorway to Nanoscle Physics* (*Lecture Notes in Physics* vol 667) ed W D Heiss

[3] Wendin G and Shumeiko V S 2006 Superconducting circuits, qubits and computing *Handbook of Theoretical and Computational Nanotechnology* ed M Rieth and W Schommers (Los Angeles: American Scientific) chapter 129
Wendin G and Shumeiko V S *Preprint* cond-mat/0508729

[4] Roos C F, Lancaster G P T, Riebe M, Häffner H, Hänsel W, Gulde S, Becher C, Eschner J, Schmidt-Kaler F and Blatt R 2004 Bell states of atoms with ultralong lifetimes and their tomographic state analysis *Phys. Rev. Lett.* **92** 220402

[5] Riebe M *et al* 2004 Deterministic quantum teleportation with atoms *Nature* **429** 734

[6] Barrett M D *et al* 2004 Deterministic quantum teleportation of atomic qubits *Nature* **429** 737

[7] Chiaverini J *et al* 2004 Realization of quantum error correction *Nature* **432** 602

[8] Leibfried D *et al* 2005 Creation of a six-atom 'Schrödinger cat' state *Nature* **438** 639

[9] Häffner H *et al* 2005 Scalable multiparticle entanglement of trapped ions *Nature* **438** 643

[10] Blais A, Huang R-S, Wallraff A, Girvin S M and Schoelkopf R J 2004 Cavity quantum electrodynamics for superconducting electrical circuits: an architecture for quantum computation *Phys. Rev.* A **69** 062320

[11] Rau I, Johansson G and Shnirman A 2004 Cavity QED in superconducting circuits: susceptibility at elevated temperatures *Phys. Rev.* B **70** 054521

[12] Wallraff A, Schuster D, Blais A, Frunzo L, Huang R-S, Majer J, Kumar S, Girvin S M and Schoelkopf R J 2004 Cavity quantum electrodynamics: coherent coupling of a single photon to a Cooper pair box *Nature* **431** 165

[13] Quantum information processing and communications fet proactive initiative in the 6th Framework Programme Strategic Report http://www.cordis.lu/ist/fet/qipc.htm

[14] ARDA Quantum Computation Roadmap http://qist.lanl.gov/

[15] Sillanpää M A, Lehtinen T, Paila A, Makhlin Yu, Roschier L and Hakonen P J 2005 *Phys. Rev. Lett.* **95** 206806

[16] Duty T, Johansson G, Bladh K, Gunnarsson D, Wilson C and Delsing P 2005 Observation of quantum capacitance in the Cooper-pair transistor *Phys. Rev. Lett.* **95** 206807

[17] Zorin A 2002 Cooper pair qubit and electrometer in one device *Physica* C **368** 284

[18] Il'ichev E, Oukhanski N, Izmalkov A, Wagner Th, Grajcar M, Meyer H-G, Smirnov A Yu, van den Brink A M, Amin M H S and Zagoskin A M 2003 Continuous monitoring of Rabi oscillations in a Josephson flux qubit *Phys. Rev. Lett.* **91** 097906

[19] Sillanpää M, Roschier L and Hakonen P 2004 The inductive single-electron transistor (L-SET) *Phys. Rev. Lett.* **93** 066805

[20] Lupascu A, Harmans C J P M and Mooij J E 2005 State detection of a superconducting flux qubit using a dc-SQUID in the inductive mode *Phys. Rev.* B **71** 184506

[21] Bertet P, Chiorescu I, Harmans C J P M and Mooij J E 2005 Dephasing of a flux qubit coupled to a harmonic oscillator *Preprint* cond-mat/0507290

[22] Makhlin Y, Schön G and Shnirman A 2001 Quantum state engineering with Josephson-junction devices *Rev. Mod. Phys.* **73** 357
[23] Wilhelm F K 2003 An asymptotical von-Neumann measurement strategy for solid-state quantum bits *Phys. Rev.* **68** 060503(R)
[24] Nakamura Y, Pashkin Yu and Tsai J S 1999 Coherent control of macroscopic quantum states in a single-Cooper-pair box *Nature* **398** 786
[25] Duty T, Gunnarsson D, Bladh K and Delsing P 2004 Coherent dynamics of a charge qubit *Phys. Rev.* B **69** 1405023(R)
[26] Schoelkopf R J, Wahlgren P, Kozhevnikov A A, Delsing P and Prober D E 1998 The radio-frequency single-electron transistor (rf-SET): a fast and ultra-sensititive electrometer *Science* **280** 1238
[27] Astafiev O, Pashkin Yu A, Yamamoto T, Nakamura Y and Tsai J S 2004 Single-shot measurement of the Josephson charge qubit *Phys. Rev.* B **69** 180507(R)
[28] Vion D, Cottet A, Aassime A, Joyez P, Pothier H, Urbina C, Esteve D and Devoret M H 2002 Manipulating the quantum state of an electrical circuit *Science* **296** 886
[29] Vion D, Aassime A, Cottet A, Joyez P, Pothier H, Urbina C, Esteve D and Devoret M H 2003 Rabi oscillations, Ramsey fringes and spin echoes in an electrical circuit *Fortsch. Phys.* **51** 462
[30] Corlevi S, Guichard W, Hekking F W J and Haviland D B 2005 Phase-charge duality of a Josephson junction in a fluctuating electromagnetic environment *Preprint* cond-mat/0510504
[31] Sjostrand J, Walter J, Tholen E, Hansson H, Haviland D and Karlhede A 2005 Phase space topology of a switching current detector *Preprint* cond-mat/0510246
[32] Mooij J E, Orlando T P, Levitov L, Tian L, van der Wal C H and Lloyd S 1999 Josephson persistent current qubit *Science* **285** 1036
[33] van der Wal C H, ter Haar A C J, Wilhelm F, Schouten R N, Harmans C J P M, Orlando T P, Lloyd S and Mooij J E 2000 Quantum superposition of macroscopic persistent-current states *Science* **290** 773
[34] Friedman J R, Patel V, Chen W, Tolpygo S K and Lukens J E 2000 Detection of a Schrödinger's cat state in an rf-SQUID *Nature* **406** 43
[35] Chiorescu I, Nakamura Y, Harmans C J P M and Mooij J E 2003 Coherent quantum dynamics of a superconducting flux-qubit *Science* **299** 1869
[36] Chiorescu I, Bertet P, Semba K, Nakamura Y, Harmans C J P M and Mooij J E 2004 Coherent dynamics of a flux qubit coupled to a harmonic oscillator *Nature* **431** 159
[37] Aassime A, Gunnarsson D, Bladh K, Delsing P and Schoelkopf R 2001 Radio-frequency single-electron transistor: toward the shot-noise limit *Appl. Phys. Lett.* **79** 4031
[38] Aassime A, Johansson G, Wendin G, Delsing P and Schoelkopf R 2001 Radio-frequency single-electron transistor as read-out device for qubits: charge sensitivity and back-action *Phys. Rev. Lett.* **86** 3376
[39] Johansson G, Käck A and Wendin G 2002 Single shot charge qubit read-out using a single electron transistor: back-action and fidelity *Phys. Rev. Lett.* **88** 046802
[40] Käck A, Wendin G and Johansson G 2003 Full frequency voltage noise spectral density of a single electron transistor *Phys. Rev.* B **67** 035301
[41] Astafiev O, Pashkin Yu A, Nakamura Y, Yamamoto T and Tsai J S 2004 Quantum noise in the Josephson charge qubit *Phys. Rev. Lett.* **93** 267007
[42] Ithier G *et al* 2005 Decoherence in a superconducting quantum bit circuit *Phys. Rev.* B **72** 134519
[43] Büttiker M 1987 Zero-current persistent potential drop across small-capacitance Josephson junctions *Phys. Rev.* B **36** 3548
[44] Bouchiat V, Vion D, Joyez P, Esteve D and Devoret M H 1998 Quantum coherence with a single cooper pair *Phys. Scr.* T **76** 165
[45] Widom A, Megaloudis G, Clark T D, Mutton J E, Prance R J and Prance H 1984 The Josephson pendulum as a nonlinear capacitor *J. Low Temp. Phys.* **57** 651
[46] Averin D V, Zorin A B and Likharev K K 1985 Bloch oscillations in small Josephson junctions *Sov. Phys.—JETP* **61** 407
[47] Likharev K K and Zorin A B 1985 Theory of the Bloch-wave oscillations in small Josephson junctions *J. Low Temp. Phys.* **59** 347
[48] Johansson G, Tornberg L and Wilson C 2006 Quantum efficient charge qubit read-out, in preparation
[49] Yurke B and Denker J S 1984 Quantum network theory *Phys. Rev.* A **29** 1419–37
[50] Devoret M 1997 Quantum fluctuations in electrical circuits *Les Houches Session LXIII, 1995, Quantum Fluctuations* ed S Reynaud, E Giacobino and J Zinn-Justin (Amsterdam: Elsevier)
[51] Barnett S M and Radmore P M 1997 *Methods in Theoretical Quantum Optics* (New York: Oxford University Press)

[52] Gardiner C W and Zoller P 1991, 2000 *Quantum Noise, A Handbook of Markovian and Non-Markovian Quantum Stochastic Methods with Applications to Quantum Optics* (Berlin: Springer)
[53] Wallraff A, Schuster D I, Blais A, Frunzio L, Majer J, Devoret M H, Girvin S M and Schoelkopf R J 2005 Approaching unit visibility for control of a superconducting qubit with dispersive readout *Phys. Rev. Lett.* **95** 060501
[54] Burkard G 2004 Theory of solid state quantum information processing *Handbook of Theoretical and Computational Nanotechnology* (*Preprint* cond-mat/0409626)
[55] Takayanagi H, Tanaka H, Saito S and Nakano H 2003 Readout of the qubit state with a dc-SQUID *Superlatt. Microstruct.* **32** 221
[56] Staf M 2003 Quantum mechanics of superconducting circuits *Master Thesis* Göteborg
[57] Barone A and Paterno G 1982 *Physics and Applications of the Josephson Effect* (New York: Wiley)